RSC Advances

PAPER

View Article Online
View Journal | View Issue



Cite this: *RSC Adv.*, 2017, **7**, 42529

# The structural, electronic and catalytic properties of $Au_n$ ($n = 1–4$) nanoclusters on monolayer $MoS_2$

Hui Zhang,[a] Jia Zhu,*[a] Hongge Zhang,[a] Jinyan Zhang,[a] Yongfan Zhang[bc] and Zhang-Hui Lu*[a]

The structural stability, electronic and catalytic properties of $Au_n$ ($n = 1–4$) nanoclusters supported on monolayer $MoS_2$ have been investigated based on first principle DFT calculation with van der Waals (vdW) corrections. Our results show that all $Au_n$ ($n = 1–4$) nanoclusters prefer to bind vertically on the top S sites of the monolayer $MoS_2$. And the relative stability of $Au_n$ ($n = 1–4$) clusters in gas phase is not preserved after landing on monolayer $MoS_2$. By including van der Waals (vdW) corrections with different approaches, we found that the van der Waals correction increased the adsorption energies for all supported $Au_n$ ($n = 1–4$) clusters with the order of $E_{ads}$(PBE-D2) > $E_{ads}$(PBE-D3) > $E_{ads}$(optB86b-vdW) > $E_{ads}$(PBE). And the van der Waals effects can also change the order of stability and the energy differences of various deposition configurations. In addition, the binding of $O_2$ is also modeled, showing significantly enhanced adsorption properties and catalytic activation toward $O_2$ adsorption, especially for that on supported $Au_1$ and $Au_3$ clusters with magnetic properties, with respect to that on supported $Au_2$ and $Au_4$ clusters with nonmagnetic properties. The current study provides further insight into the adsorption and catalytic properties of small gold clusters supported on monolayer $MoS_2$, which play a crucial role in the activation of $O_2$.

Received 10th July 2017
Accepted 29th August 2017

DOI: 10.1039/c7ra07591j

rsc.li/rsc-advances



## 1 Introduction

Supported gold nanoclusters have attracted considerable interest due to their unexpected catalytic properties in contrast with the inactivity of larger-sized particles or bulk gold.[1,2] In the past few years, they have been widely applied in heterogeneous catalysis field to catalyze many reactions, such as low temperature CO oxidation,[3–5] water-gas shift (WGS) reaction[6,7] and the oxidation of alkenes.[8] It is revealed that the chemical properties and catalytic activity of supported gold nanoclusters are dramatically depended by the size and shape of gold nanoclusters,[9–12] the structural fluxionality,[13–15] and the forms of the supported materials.[10,16–18] Recent experimental and theoretical works have focused on the effects of support materials on modifying/activating Au clusters by comparing various substrates including MgO,[18] $TiO_2$,[19] $SiO_2$,[20] $CeO_2$,[21] and $Fe_2O_3$.[22] In particular, it is demonstrated that the different charged gold cluster is one of the origins for the high catalytic activity of supported gold nanoclusters. Well characterized examples are those of negative charged gold nanoclusters forming when gold clusters deposited on $TiO_2$, defect MgO and $CeO_2$, result in activation of $O_2$ molecules for further catalytic reaction or dissociation.[18,20,21] On the other hand, after adsorption on $Fe_2O_3$ and $SiO_2$ surface the gold nanoclusters become positive charged, which promote adsorption of other reactants, such as CO and hydrocarbons.[20,22,23] It is indicated that the catalytic activity of gold clusters are strongly influenced by the types of support materials. Therefore, the choice of suitable support is crucial for a rational design of chemical properties and activities of supported gold clusters.

In the past few years, a continuously increasing interest have been devoted to two-dimensional nanomaterials, such as graphene, silicene, hexagonal boron nitride (h-BN), $TiO_2$ nanosheet, serving as excellent candidates of the support of metal nanoparticles for enhancing adsorption performances and catalytic properties of metal catalysts, because of their extraordinary physical, chemical and optical properties.[24–31] For example, graphene has been shown to be an excellent substrate material for dispersion of the transition metal (TM) nanoparticles, due to its large surface areas, outstanding electronic and thermal conductivity, as well as the high mechanical strength and low production cost.[32,33] Theoretically calculation showed that supported gold clusters on h-BN surface can considerably enhance their adsorption and catalytic activity of adsorbed $O_2$ molecule.[28] On the other hand, the great advance in two-dimensional-based nanomaterials research has encouraged scientists to explore other two-dimension-based materials. Among them, one emerging class of transition metal

[a]College of Chemistry and Chemical Engineering, Jiangxi Normal University, Nanchang, Jiangxi 330022, China. E-mail: jia_zhu@jxnu.edu.cn; luzh@jxnu.edu.cn
[b]Department of Chemistry, Fuzhou University, Fuzhou, Fujian, 350108, China
[c]State Key Laboratory of Photocatalysis on Energy and Environment, Fuzhou, Fujian, 350002, China

dichalcogenides (TMDs), monolayer molybdenum disulfide ($MoS_2$) has been a recent hot topic. Indeed, monolayer $MoS_2$ is a semiconductor with a direct band gap of 1.9 eV,[34] which are associated with large surface areas and abundant active sites.[35,36] The experimental results from Xia *et al.* suggested that Au nanorods deposited on $MoS_2$ nanosheets activates the electrocatalytic activity for hydrogen evolution reaction (HER).[37] However, very little attention has been paid to theoretical investigation concerning the role of the $MoS_2$ support on the chemical and catalytic properties of gold nanoparticles. The structural, electronic properties, and catalytic activation of supported gold clusters on monolayer $MoS_2$ are also not obtained, which is very essential for investigating the cluster-support interaction effects, interface structure, as well as the charge transfer between supported gold cluster and substrate. In addition, van der Waals (vdW) forces are ubiquitous in the binding of atoms and molecules. In the past few years accurately accounting for van der Waals (vdW) forces and understanding the role they play in extended systems have become a thriving topic of research, which play a crucial role in improvement of theoretical description for those systems.[34,38,39]

In this work, by performing first principles DFT, we investigate the structures and electronic properties of $Au_n$ ($n = 1$–4) clusters supported on monolayer $MoS_2$ including the van der Waals (vdW) forces correction. Furthermore, to further understand the modification/activation of gold nanoclusters on monolayer $MoS_2$, the adsorption behaviors of $O_2$ on $Au_n$ ($n = 1$–4)/$MoS_2$ are also determined. The paper is organized as follows. We first study the gas-phase $Au_n$ ($n = 1$–4) clusters. Then, we investigate the structures and electronic properties of $Au_n$ ($n = 1$–4) clusters supported on monolayer $MoS_2$ with DFT results. Furthermore, the effects of the van der Waals corrections using several vdW inclusive DFT schemes (PBE-D2, PBE-D3 and optB86b-vdW) are discussed. Finally, we discussed the adsorption and activation behaviors of $O_2$ molecule on $Au_n$ ($n = 1$–4)/$MoS_2$ systems, which can help for further insight into adsorption and catalysis properties of small gold clusters supported on monolayer $MoS_2$.

## 2 Computational details

Spin-polarized density functional theory (DFT) calculations were performed using the Vienna Ab initio Simulation Package (VASP)[40–42] and the projected augmented wave (PAW) methods.[43,44] The generalized gradient approximation of Perdew, Burke and Ernzerhof (PBE) functional[45] was employed to treat the exchange-correlation energy of interaction electrons. The kinetic energy cutoff for the plane-wave expansion was set to 400 eV. A ($3 \times 3 \times 1$) Monkhorst–Pack (MP) mesh was used for the *k*-point sampling of the Brillouin zone. To calculate the projected density of states (PDOS), the set of *k*-points was adjusted to ($5 \times 5 \times 1$). The lattice parameter of monolayer $MoS_2$ was optimized to be 3.18 Å, which is in good agreement with the experimental (3.20 Å [46]) and theoretical values (3.18 Å,[47,48] 3.19 Å,[49] 3.20 Å [50]). To accommodate various sizes of the gold clusters, a ($5 \times 5$) supercell consisting of 75 atoms (50 S atoms and 25 Mo atoms) was introduced. The supercell size of the monolayer $MoS_2$ has been tested and the ($5 \times 5$) supercell is large enough to obtain the properties focused on the present work. During the geometry optimization all the atoms in the monolayer $MoS_2$ were relaxed in all directions.

For $Au_1$ and $Au_2$ clusters, we started by placing the $Au_1$ and $Au_2$ clusters on different sites of monolayer $MoS_2$ as different adsorption models. Then these initial geometries were optimized using above settings. Since the ground states of $Au_3$ and $Au_4$ clusters in gas phase are V-shaped[51] and rhombic[52] structures, respectively. We first place these two clusters on the monolayer $MoS_2$ as initial structures. The deposition of $Au_3$ and $Au_4$ clusters on the monolayer $MoS_2$ are more complicated with many possible arrangements of the supported clusters on monolayer $MoS_2$. Therefore, we performed *ab initio* MD simulations using the Nosé algorithm[53] with a cutoff energy of 200 eV to explore possible structures of the $Au_3$ and $Au_4$ clusters deposition on monolayer $MoS_2$. The simulation length was 10 ps with a time step of 1 fs at the temperature of 600 K. Then, some possible deposition configurations were sampled from the results of the MD simulations every 50 steps, result in 200 initial configurations for each MD process. Further structural optimizations using more accurate settings (see above) were performed to determine the typical stable configurations. Similar approaches have been employed to investigate other complicated systems, including $CrW_2O_9$/MgO(001),[54,55] Au/$TiO_2$ and Au/$ZrO_2$(101).[38]

The role of the van der Waals correction was investigated using three vdW correction methods as follows: DFT-D2 [56] and DFT-D3 [57] with pairwise force field method proposed by Grimme and co-workers. The optB86b-vdW method proposed by Lundqvist and co-workers, in which the vdW contribution is expressed directly as a function of the electron density.[58] In addition to van der Waal correction which is crucial to well describe the interaction between the cluster and substrate at the interface, the electronic structures for the adsorbed $Au_n$ clusters may be affected by the onsite correction to the strong correlated d electrons. Actually, test calculations using GGA + U method combined with projected augmented wave (PAW) were also performed, and our results indicated that GGA and GGA + U methods yielded similar results of configurations and electronic structure including total of Bader charge, the atomic Bader charge of adsorbed $Au_n$ cluster, total magnetization, the total DOSs and particle DOSs projected on the S 3p, Mo 4d, Au 6s and 5d orbitals in the present work.

## 3 Results and discussion

### 3.1 Structures of $Au_n$ ($n = 1$–4) clusters in the gas phase

Before considering the cases of supported gold clusters, we first discuss the structures of $Au_n$ ($n = 1$–4) clusters in gas phase. Many experimental[59–64] and theoretical works[51,52,65–67] have been devoted to the structures and stability of gold clusters. Schaaff *et al.*[60] have isolated five massive gold-cluster molecules in high yield and the electronic structure of these molecules has been deduced by optical absorption spectroscopy. Zanti *et al.*[51] have obtained the structures of small gold clusters $Au_n$ ($n \leq 16$) using density functional theory at B3LYP level. Lee *et al.*[52] further explore the relative stabilities and electronic properties of small

 

neutral and anionic gold clusters ($Au_n$ and $Au_n^-$, $n = 4$–7) using high-level CCSD(T) calculations with large basis sets. In here, the geometry and the stability of $Au_n$ ($n = 1$–4) clusters (placed in a 20 × 20 × 20 Å cubic box) are reexamined at the PBE level with a plane-wave basis set. The calculated structures of ground state and low-lying isomers with corresponding structural parameters and relative energies are shown in Fig. 1. For $Au_2$ cluster (Fig. 1b), the calculated Au–Au bond length is 2.53 Å, which is in agreement with the reported experimental value (2.47 Å).[68] For $Au_3$ cluster, there are two low-lying isomers. Fig. 1c shows that the ground state of $Au_3$ cluster is V-shaped structure ($C_{2v}$ symmetry) with two Au–Au bonds (2.56 Å) and the bond angle of 137.7°. Other $Au_3$ isomer (Fig. 1d) is triangular geometry with $D_{3h}$ symmetry, which is 0.11 eV higher in energy than that of the V-shaped $Au_3$ cluster. Each Au–Au bond length of the equilateral triangle $Au_3$ cluster is 2.67 Å. The order of the stability for the $Au_3$ cluster is consistent with that obtained by Zanti *et al.* using B3LYP method with an atomic orbital basis set.[51] In the case of $Au_4$ cluster, there are four low-lying isomers: rhombic $Au_4$, Y-shaped $Au_4$, zigzag $Au_4$ and tetrahedral $Au_4$. The ground state of $Au_4$ cluster (Fig. 1e) is rhombic with $C_s$ symmetry. The bond lengths of Au–Au bonds at four side of rhombic $Au_4$ cluster are all 2.69 Å and the length of diagonal Au–Au bond is 2.63 Å. The second low-lying isomer (Fig. 1f) is Y-shaped structure ($C_{2v}$ symmetry), which is just 0.04 eV higher in energy than that of the rhombic $Au_4$ cluster. The calculated order of the stability for rhombic $Au_4$ and Y-shaped $Au_4$ is in agreement with the result at CCSD(T) level reported by Lee *et al.*[52] While the third low-lying $Au_4$ isomer (Fig. 1g) is Zigzag structure with $C_s$ symmetry, whose energy is 0.41 eV higher than that of the ground state of $Au_4$ cluster. It can be seen that rhombic $Au_4$ cluster, Y-shaped $Au_4$ cluster and Zigzag $Au_4$ cluster are separated just by small energy differences. Thus, it can be expected that the interconversion of one isomer into another may occur among the three low-lying isomers of $Au_4$ cluster. The fourth $Au_4$ isomer with highly symmetric $T_d$ tetrahedral structure (Fig. 1h) has also been considered. It is the first occurring of 3D geometry of gold clusters. However, it is unstable in consequence of Jahn–Teller distortions, significantly 1.27 eV in energy higher with respect to the ground state of $Au_4$ cluster.

### 3.2 Structures of $Au_n$ ($n = 1$–4) clusters supported on monolayer $MoS_2$

**3.2.1 DFT-PBE adsorption results without vdW interactions.** The deposition configurations of $Au_n$ ($n = 1$–4) clusters on monolayer $MoS_2$ at the PBE level are shown in Fig. 2. For the deposition of Au atom on monolayer $MoS_2$ (Fig. 2a), we found that Au atom preferentially interacts with monolayer $MoS_2$ at the S-top site with the bond length of 2.37 Å, and the corresponding adsorption energy is 0.63 eV. For $Au_2$ cluster supported on monolayer $MoS_2$ (Fig. 2b), it can be seen that $Au_2$ cluster also prefers to bind vertically on the S-top sites of the monolayer $MoS_2$ *via* one Au atom. The bond distance of S–Au bond is 2.30 Å, which is shorter than that in $Au_1/MoS_2$ system (2.37 Å), suggesting the stronger interaction between the $Au_2$ cluster and monolayer $MoS_2$. Not surprisingly, corresponding adsorption energy of the supported $Au_2$ cluster on monolayer $MoS_2$ (1.02 eV) is 0.39 eV higher in energy than that of supported Au atom. While for $Au_3$ cluster supported on monolayer $MoS_2$, we notice that $Au_3$ cluster assumes two different structures (Fig. 2c and d). In the first configuration M1 (Fig. 2c), after adsorption on monolayer $MoS_2$, the $Au_3$ cluster completely loses the initial V-shaped structure in gas phase and forms a triangular structure taking a vertical orientation. The triangular $Au_3$ cluster is bound to the surface with two Au atoms coordinated to two S atoms, respectively, with average bond lengths of 2.36 Å. And the corresponding adsorption energy is 1.37 eV. In contrast, in model M2 (Fig. 2d), the supported $Au_3$ cluster maintains the V-shaped structure in gas phase. In this structure, two terminal Au atoms in V-shaped $Au_3$ cluster bind to two surface S atoms with vertical deposition mode. The average bond length of the two Au–S bonds (2.38 Å) is 0.02 Å longer than that of model M1, indicating weaker Au–S bonds compared with that of model M1. The adsorption energy is 1.31 eV. At the PBE level, the energy difference between the model M1 and M2 is no more than 0.06 eV. While for the case of $Au_4/MoS_2$ systems, the deposition structures are more complicated, the ground state and low-lying structures within 0.50 eV are presented in Fig. 2e–g. In model M1 (Fig. 2e), the $Au_4$ cluster loses initial rhombic structure in gas phase and forms a Y-shaped geometry. The Y-shaped $Au_4$ cluster is vertically supported on monolayer $MoS_2$ by forming two Au–S bonds with the bond lengths of

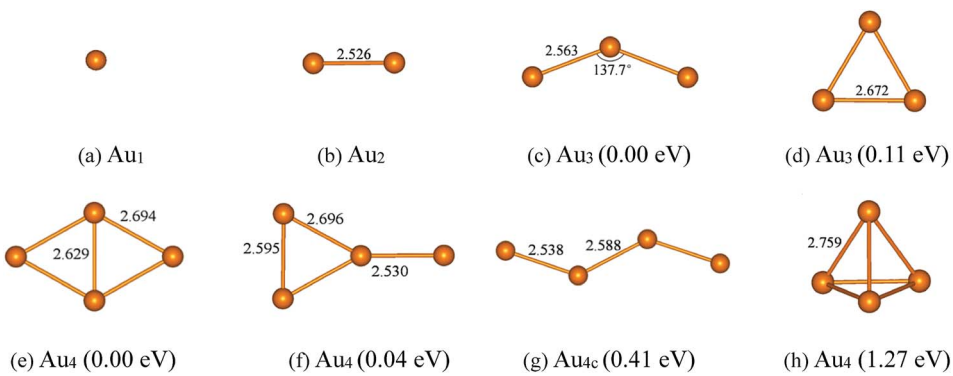


Fig. 1 The optimized structures and their relative energies of $Au_n$ ($n = 1$–4) clusters. Selected bond lengths are given in angstroms and bond angles in degrees.

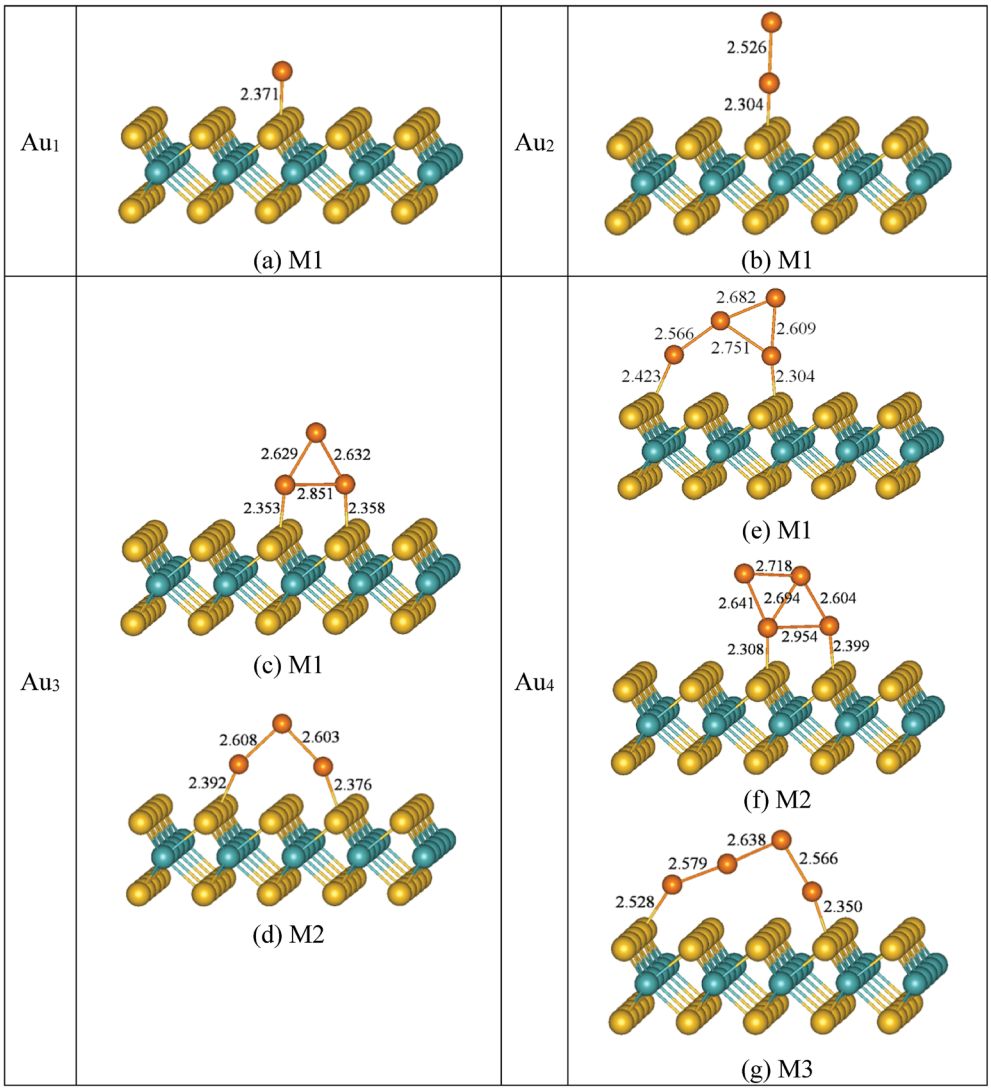


Fig. 2 Optimized structures of $Au_n$ ($n = 1$–4) clusters adsorption on monolayer $MoS_2$. Color coding: orange, Au atoms; yellow, S atoms; cyan, Mo atoms. Selected bond lengths are given in angstroms.

2.42 Å and 2.30 Å, respectively. In the model M2 (Fig. 2f), after the $Au_4$ cluster deposition on monolayer $MoS_2$, the rhombic structure of $Au_4$ cluster in gas phase is maintained. Two neighbouring Au atoms are bonded to two surface S atoms with bond lengths of 2.31 Å and 2.40 Å, respectively. While for model M3, unlike the M1 and the M2, after deposited on the monolayer $MoS_2$, the $Au_4$ cluster is distorted and elongated, resulting in linear configuration. The linear $Au_4$ cluster is also vertically adsorbed on monolayer $MoS_2$ by two terminal Au atoms bound with two surface S atoms with the bond lengths of 2.53 Å and 2.35 Å, respectively. Moreover, a three-dimensional supported structure with a tetrahedral shape is also investigated. We found that it is unstable on monolayer $MoS_2$. This is true at all levels of theory considered (with and without vdW forces). This phenomenon has been reported for $Au_4$ cluster on $TiO_2$ and $ZrO_2(101)$ surface.[38] Now let us discuss the relative stabilities of above three deposition configurations for $Au_4/MoS_2$ systems. The adsorption energies of the three structures are listed in Table 1. The model M1 is preferred ($E_{ads} = 1.48$ eV) compared to M2 and M3. The model M2 with the adsorption energy of 1.39 eV is only 0.09 eV higher in energy than that of model M1. While for model M3 ($E_{ads} = 0.99$ eV), it is the most unstable structure, which is 0.49 eV and 0.40 eV higher in energy than that in model M1 and M2, respectively. It is clear that the M1 which is originated from the unstable $Au_4$ isomer in gas phase (Fig. 1f) shows the best thermodynamical stability, while the M2 model which is derived with the most stable cluster in gas phase (Fig. 1e) now is higher in energy (0.09 eV) than M1. Therefore, the relative stability of $Au_4$ isomer in gas phase is exchanged after depositing on the monolayer $MoS_2$, indicating a possible way to stabilize the unstable clusters in the gas phase by choosing a suitable support from a thermodynamical point of view.

**3.2.2 Adsorption results with vdW interaction.** Next, we will discuss the effects of van der Waals forces for the adsorption of $Au_n$ ($n = 1$–4) clusters on monolayer $MoS_2$ using several vdW

 

Table 1 Adsorption energy ($E_{ads}$) and the average bond length of Au–S bond ($\bar{d}$(Au–S)) for $Au_n$ ($n = 1$–4) clusters deposited on monolayer $MoS_2$ with and without the inclusion of van der Waals forces

| | | $E_{ads}$[a] (eV) | | | | $\bar{d}$ (Au–S) (Å) | | | |
|---|---|---|---|---|---|---|---|---|---|
| | | PBE | PBE-D2 | PBE-D3 | optB86b-vdW | PBE | PBE-D2 | PBE-D3 | optB86b-vdW |
| $Au_1/MoS_2$ | M1 | 0.63 | 1.23 | 1.07 | 0.97 | 2.37 | 2.31 | 2.33 | 2.35 |
| $Au_2/MoS_2$ | M1 | 1.02 | 1.76 | 1.56 | 1.41 | 2.30 | 2.25 | 2.27 | 2.29 |
| $Au_3/MoS_2$ | M1 | 1.37 | 2.69 | 2.36 | 2.14 | 2.36 | 2.29 | 2.32 | 2.34 |
| | M2 | 1.31 | 2.80 | 2.39 | 2.13 | 2.38 | 2.33 | 2.35 | 2.37 |
| $Au_4/MoS_2$ | M1 | 1.48 | 3.09 | 2.67 | 2.29 | 2.36 | 2.30 | 2.33 | 2.35 |
| | M2 | 1.39 | 2.91 | 2.51 | 2.17 | 2.35 | 2.27 | 2.31 | 2.33 |
| | M3 | 0.99 | 2.82 | 2.33 | 1.90 | 2.44 | 2.37 | 2.40 | 2.42 |

[a] The $E_{ads}$ in this table is defined as $E_{ads} = E_{MoS_2(001)} + E_{Au_n(n=1\text{–}4)\ clusters} - E_{Au_n/MoS_2}$, where $E_{MoS_2}$, $E_{Au_n(n=1\text{–}4)\ clusters}$, $E_{Au_n/MoS_2}$ and $n$ represent the total energies of the monolayer $MoS_2$, the ground states of $Au_n$ ($n = 1$–4) clusters in the gas phase, the entire systems after depositing $Au_n$ ($n = 1$–4) clusters on monolayer $MoS_2$ and the number of metal atoms in the cluster, respectively.

inclusive DFT schemes (PBE-D2, PBE-D3 and optB86b-vdW). It can be seen that the structures change only slightly after inclusion of vdW forces, with the largest difference being of 0.08 Å. As displayed in Table 1 and Fig. 3, we found that the van der Waals correction increased the adsorption energies for all $Au_n$ ($n = 1$–4)/$MoS_2$ systems with the relative order of adsorption energies of $E_{ads}$(PBE-D2) > $E_{ads}$(PBE-D3) > $E_{ads}$(optB86b-vdW) > $E_{ads}$(PBE). It can be seen clearly that there is a trend that the PBE-D2 method provides the largest correction to the strength of dispersion interactions, whereas optB86b-vdW gives the smallest. For Au atom deposition on the monolayer $MoS_2$, the adsorption energy goes from 0.63 eV (PBE) to 1.23 eV (PBE-D2), 1.07 eV (PBE-D3), and 0.97 eV (optB86b-vdW), with the relative order of $E_{ads}$(PBE-D2) > $E_{ads}$(PBE-D3) > $E_{ads}$(optB86b-vdW) > $E_{ads}$(PBE). Like the Au atom, the same trend can also be found for $Au_2/MoS_2$ system, the PBE-D2 method gives the largest vdW correction with the adsorption energy of 1.76 eV and optB86b-vdW gives the smallest (1.41 eV), while PBE-D3 method gives the value of adsorption energy (1.56 eV) located just between PBE-D2 method and optB86b-vdW method. Considering supported $Au_3$ cluster, the inclusion of the vdW forces has a stronger effect on the $Au_3/MoS_2$ systems with the shorter bond distance of Au–S bond. Therefore, the adsorption energy is much increased, for model M1 from 1.37 eV (PBE) to 2.69 eV (PBE-D2), 2.36 eV (PBE-D3), and 2.14 eV (optB86b-vdW), and for model M2 from 1.31 eV (PBE) to 2.80 eV (PBE-D2), 2.39 eV (PBE-D3) and 2.13 eV (vdW-DF), with an increase in the adsorption energies of around 56% – 114%. In addition, interestingly, compared with PBE results, the order of stability of model M1 and M2 at the PBE-D2 and PBE-D3 levels is changed. At PBE level the preferred structure is the triangular shape, the model M1, whereas at PBE-D2 and PBE-D3 levels the preferred structure becomes the V-shaped, model M2. However, there is no change in the order of stability of the two low-lying structures for $Au_3/MoS_2$ systems at vdW-DF level. This effect is not observed for Au atom and $Au_2$ deposition on the monolayer $MoS_2$. While for $Au_4/MoS_2$ systems, when the long-range terms are included, the adsorption energies are increased with the relative order of $E_{ads}$(PBE-D2) > $E_{ads}$(PBE-D3) > $E_{ads}$(optB86b-vdW) > $E_{ads}$(PBE), in line with the results obtained from other $Au_n$ ($n = 1$–3) clusters on monolayer $MoS_2$. Differently from $Au_3/MoS_2$ systems, the order of stability of $Au_4/MoS_2$ systems is maintained with the order of M1 > M2 > M3. But the energy difference among the three structures has changed. Once vdW contributions are considered, the energy difference between M1 and M2 becomes larger (0.18 eV, 0.16 eV and 0.12 eV at PBE-D2, PBE-D3 and optB86b-vdW level, respectively, *versus* 0.09 eV at PBE level). Whereas energy difference between M1 and M3 becomes smaller (0.27 eV, 0.34 eV and 0.39 eV at PBE-D2, PBE-D3 and vdW-DF level, respectively, *versus* 0.49 eV at PBE level).

To summarize, for $Au_n$ ($n = 1$–4) clusters on monolayer $MoS_2$, we observed that the geometric structures change only slightly after inclusion of vdW forces, the largest difference being of 0.08 Å. While the van der Waals effects make the major corrections to the adsorption energies, with the relative order of $E_{ads}$(PBE-D2) > $E_{ads}$(PBE-D3) > $E_{ads}$(optB86b-vdW) > $E_{ads}$(PBE). The PBE-D2 method provides the largest correction to the strength of dispersion interactions, whereas optB86b-vdW gives the smallest. After inclusion of the van der Waals correction, it can also change the order of relative stability and the energy differences of various deposition configurations.

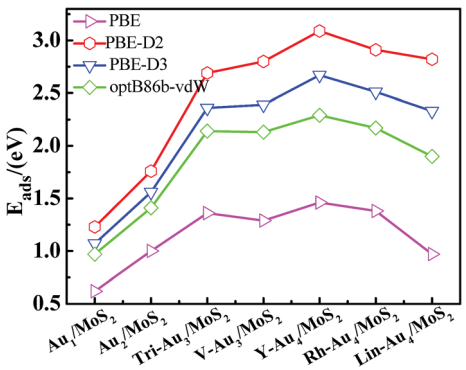


Fig. 3 The adsorption energies of supported $Au_n$ ($n = 1$–4) clusters obtained at PBE, DFT-D2, DFT-D3 and optB86b-vdW (pink, red, dark blue and green polylines, respectively).

### 3.3 Electronic structures of $Au_n$ ($n$ = 1–4) clusters supported on monolayer $MoS_2$

To better investigate the effects introduced by the deposition of $Au_n$ ($n$ = 1–4) clusters on the monolayer $MoS_2$, in this section, we will focus on the electronic structures of $Au_n$ ($n$ = 1–4)/$MoS_2$ systems. The density of state (DOS) curves displayed in Fig. 4 are the individual spin-up and spin-down densities of states obtained from the spin-polarized calculations at the PBE level, which are almost the same with and without vdW contributions.

**3.3.1 Density of states (DOS).** Fig. 4a and b displayed the total DOSs and Partial DOSs projected on the S 3p and Mo 4d orbital for the clean monolayer $MoS_2$, it can be seen that monolayer $MoS_2$ is a semiconductor in which the valence band (VB) and conduction band (CB) are dominated by S 3p and Mo 4d states, respectively. Fig. 4c presents the total density of state (TDOS) of most stable configuration for $Au_1/MoS_2$ system. A distinct feature is that a spin-up peak appears near the Fermi level and a spin-down peak occurs at higher energy (about 0.37 eV) in the band gap, which is significantly different from the case on the perfect monolayer $MoS_2$. Clearly, the system of supported Au atom with odd number atom is spin polarized with the total magnetic moment of 1.0 $\mu_B$. According to the partial density of states (PDOSs) of S 3p, Mo 4d, Au 6s and 5d orbital (Fig. 4d), it is clear that the above asymmetrical peaks are mainly derived from Au 6s state. Fig. 4d also shows that the 5d state of Au atom is overlapped with S 3p state at a wide energy range (from −4.5 eV to −1 eV), indicating a strong hybridization between Au and surface S atom. Similar phenomenon is also observed for another gold cluster with odd number of atoms, $Au_3/MoS_2$ system (see Fig. 4g and h). Whereas, things are radically different in the supported gold cluster with even number of atoms. For the supported $Au_2$ cluster with even number of Au atoms, the DOS curves as shown in Fig. 4e can be seen that, differently from the supported Au and $Au_3$ atom, the most stable configuration of $Au_2/MoS_2$ system is non-spin polarized due to the closed-shell nature of the $Au_2$ cluster. An obvious characteristic is that a new symmetrical sharp feature is present near the Fermi level. Further partial density of states (PDOSs) of S 3p, Mo 4d, Au 6s and 5d orbital (Fig. 4f) show that the new peak is dominated by Au 6s and 5d states. And the electronic states of $Au_2$ cluster mixed with the top of the S 3p valence band. Similar phenomenon is also observed for another gold cluster with even number of atoms, $Au_4$ cluster supported on the monolayer $MoS_2$ (see Fig. 4i and j).

**3.3.2 Bader charges.** We further performed Bader charge analysis[69–71] to investigate the bonding nature and charge transfer at interfaces for all the adsorption systems. The results of Bader charge with and without vdW contributions are shown in Fig. 5 and summarized in Table 2. First, we discuss the Bader charges obtained by PBE method. At the PBE level, it is shown that, for the $Au_n$ ($n$ = 1, 2, 4)/$MoS_2$ system, the direction of charge transfer at the interfaces is from the substrate to the supported gold clusters. It is suggested that Au nanoclusters impose remarkable p-doping effects to the monolayer $MoS_2$, which is in good agreement with that reported in previous experiments.[72] The magnitudes of charge transfer are all small

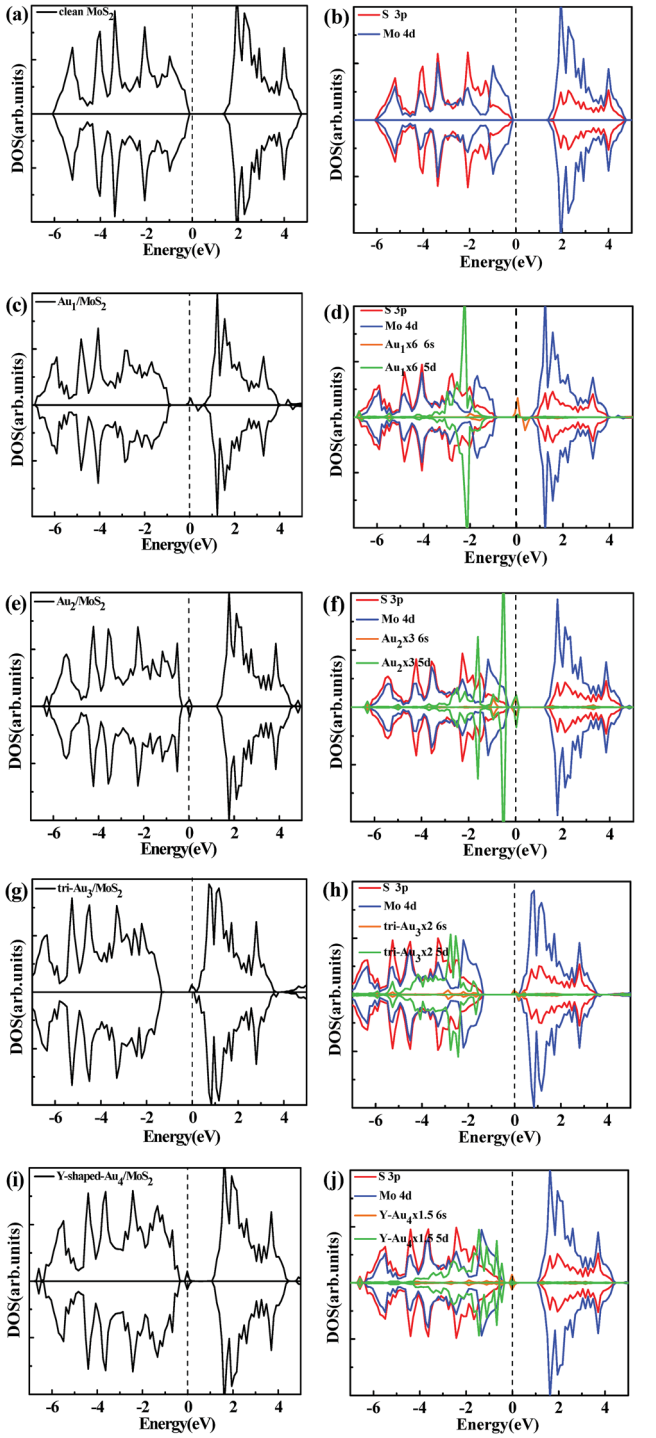


Fig. 4 Total DOSs (a) and partial DOSs projected on the S 3p and Mo 4d of the clean monolayer $MoS_2$ (b), total DOSs and partial DOSs projected on the S 3p, Mo 4d, Au 6s and 5d of the most stable configurations of $Au_1/MoS_2$ (c, d), $Au_2/MoS_2$ (e, f), typical configurations of $Au_3/MoS_2$ (g, h), and typical configurations of $Au_4/MoS_2$ (i, j). The vertical dashed line indicates the position of the Fermi level, taken as zero energy.

(<0.2$e$), which are 0.09$e$, 0.11$e$ and 0.10/0.10/0.10$e$ for supported $Au_1$, $Au_2$ and $Au_4$ clusters, respectively. While for $Au_3$ clusters supported on monolayer $MoS_2$ the magnitudes of charge

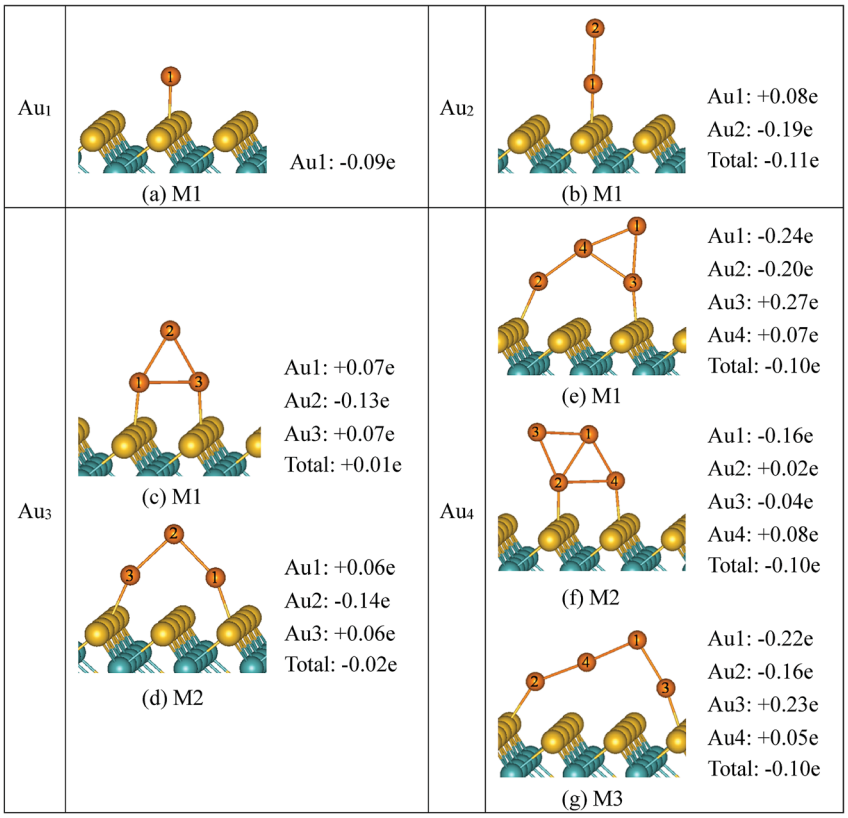


Fig. 5 The Bader charges carried by Au atoms of the supported $Au_n$ ($n$ = 1–4) clusters, at PBE level.

transfer are virtually zero. Furthermore, the charge distributions within the $Au_n$ ($n$ = 2–4) clusters are also investigated (Fig. 5). It can be seen that, although $Au_n$ ($n$ = 1–4) clusters obtained electrons or virtually zero after deposition on the monolayer $MoS_2$, the magnitudes of charge transfer are mainly obtained by the top Au atom which is far away from the monolayer $MoS_2$. Whereas most of Au atoms bonded with the surface (at the interface) become positive, which is consistent with the experimental result that hot electron is transferred from Au rods to $MoS_2$ nanosheets.[37] As shown in Fig. 5b, for $Au_2$/$MoS_2$ system, the magnitude of charge on Au(1) atom which is bound to monolayer $MoS_2$ is small and positive: $q$ = +0.08$e$, whereas the top Au atom (Au(2) atom) is negatively charged with $q$ = −0.19$e$. For $Au_3$/$MoS_2$ (Fig. 5c and d), although the charge transfers between the $Au_3$ clusters and monolayer $MoS_2$ are virtually zero, the top Au atom (Au(2) atom) holds negative charge with $q$ = −0.13/−0.14$e$, whereas the Au atoms (Au(1) atom and Au(3) atom) binding to the monolayer $MoS_2$ are positive, with $q$ = +0.07$e$/0.06$e$. In terms of the $Au_4$ clusters, the analysis of charge distributions within the $Au_4$ cluster shows that, still, there is an accumulation of charge on the top Au atoms (−0.24$e$, −0.16$e$, −0.22$e$ at M1, M2 and M3, respectively).

Table 2 The net Bader charges ($\Delta Q$) of $Au_n$ ($n$ = 1–4) clusters deposited on monolayer $MoS_2$ with and without the inclusion of van der Waals forces

| | | $\Delta Q^a$ (e) | | | |
|---|---|---|---|---|---|
| | Structures | PBE | PBE-D2 | PBE-D3 | optB86b-vdW |
| $Au_1/MoS_2$ | M1 | −0.09 | −0.11 | −0.02 | −0.05 |
| $Au_2/MoS_2$ | M1 | −0.11 | −0.15 | −0.06 | −0.09 |
| $Au_3/MoS_2$ | M1 | 0.01 | 0.02 | 0.02 | 0.00 |
| | M2 | −0.02 | −0.04 | −0.03 | −0.02 |
| $Au_4/MoS_2$ | M1 | −0.10 | −0.12 | −0.12 | −0.13 |
| | M2 | −0.10 | −0.13 | −0.15 | −0.07 |
| | M3 | −0.10 | −0.07 | −0.08 | −0.09 |

[a] The negative values indicate that the electrons are transferred from the monolayer $MoS_2$ to the $Au_n$ ($n$ = 1–4) clusters.

Table 3 Adsorption energy ($E_{ads}$) and the bond length of Au–O bond and O–O bond for $O_2$ adsorption on $Au_n$ ($n$ = 1–4)/$MoS_2$

| | $E_{ads}$[a] (eV) | $d$ (Au–O) (Å) | $d$ (O–O) (Å) |
|---|---|---|---|
| Free $O_2$ | — | — | 1.23 |
| Clean $MoS_2$ | 0.02 | — | 1.24 |
| $Au_1/MoS_2$ | 1.04 | 2.07 | 1.30 |
| $Au_2/MoS_2$ | 0.23 | 2.20 | 1.26 |
| $Au_3/MoS_2$ | 0.64 | 2.25, 2.26 | 1.32 |
| $Au_4/MoS_2$ | 0.26 | 2.21 | 1.26 |

[a] The $E_{ads}$ in this table is defined as $E_{ads} = E_{Au_n/MoS_2} + E_{O_2} - E_{O_2/Au_n/MoS_2}$, where $E_{Au_n/MoS_2}$, $E_{O_2}$, $E_{O_2/Au_n/MoS_2}$ and $n$ represent the total energies of the most stable $Au_n$ ($n$ = 1–4)/$MoS_2$ system, the ground state of $O_2$, the entire system after depositing $O_2$ on $Au_n$ ($n$ = 1–4)/$MoS_2$, and the number of metal atoms in the cluster, respectively.

The results of Bader charge with the inclusion of van der Waals are also shown in Table 2. Clearly, the inclusion of van der Waals forces has no significantly effects on the Bader charges, with the Bader charge difference always smaller than 0.07*e*.

### 3.4 Adsorption and activation of $O_2$ on $Au_n$ ($n$ = 1–4)/$MoS_2$

To study the effect of the monolayer $MoS_2$ support on the catalytic properties of the small gold clusters, we performed investigation of adsorption and activation of $O_2$ on the most stable adsorption configurations of $Au_n$ ($n$ = 1–4)/$MoS_2$ systems. Fig. 6 presents the optimized geometries of $O_2$ adsorption on $Au_n$ ($n$ = 1–4)/$MoS_2$ systems. It can be seen clearly that, for all $Au_n$ ($n$ = 1–4)/$MoS_2$ systems, $O_2$ molecule prefers to adsorb on the top Au atom of the supported gold cluster which holds main negative charge. For $O_2$ adsorption on $Au_1$/$MoS_2$ system, $O_2$ is adsorbed on the $Au_1$/$MoS_2$ system by forming one O–Au bond (2.07 Å) with the angle of 116.6° between the O–O and Au–O bonds. The O–O bond is elongated to 1.30 Å (1.23 Å in gas $O_2$ molecule), indicating activation of $O_2$ molecule. The adsorption energy is 1.04 eV. Similar results are also observed when $O_2$ adsorbed on the supported $Au_3$ cluster with odd number of Au atoms. Two O atoms are bonded with the top Au atom of supported $Au_3$ cluster which holds more negative charge, forming two Au–O bonds (2.25 Å, 2.26 Å, respectively), with the corresponding adsorption energy of 0.64 eV. After adsorption, O–O bond is elongated to 1.32 Å, indicating significantly activation of adsorbed $O_2$ molecule. Whereas, the situation is significantly different for $O_2$ adsorption on supported $Au_2$ and $Au_4$ clusters with even number of Au atoms. After adsorption, $O_2$ molecule *via* one O atom interacts with the top Au atom of the supported $Au_2$ and $Au_4$ clusters, with the bond length of Au–O bond of 2.20 Å and 2.21 Å respectively. The corresponding O–O bonds are almost not changed with the bond length of 1.26 Å compared with that in free gas $O_2$. Corresponding adsorption energy is small (0.23 eV and 0.26 eV) for $Au_2$ clusters and $Au_4$ clusters, respectively. Since there is another Au atom at the interface ($Au_2$ atom) in $Au_4$/$MoS_2$ system holds some negative charge (−0.20*e*), we also investigated the adsorption configuration when $O_2$ interacts with $Au_2$ atom which holds some negative charge. However, strong repulsive forces between surface S atoms and $O_2$ molecule make the adsorption configuration not stable (not shown).

In short, the above calculations for $O_2$ adsorption show that the adsorption energies for $O_2$ adsorption on the $Au_1$/$MoS_2$ and $Au_3$/$MoS_2$ systems with odd number of Au atoms are much higher than that on the $Au_2$/$MoS_2$ and $Au_4$/$MoS_2$ systems with even number of Au atoms (1.04 eV, 0.64 eV for Au and $Au_3$, respectively. 0.23 eV, 0.26 eV for $Au_2$ and $Au_4$, respectively), indicating stronger adsorption properties and activation for oxygen molecule on $Au_n$ ($n$ = 1, 3)/$MoS_2$ system with odd number of gold atoms. It is provide a key insight in elucidating the catalytic activity of supported gold clusters with an odd-even

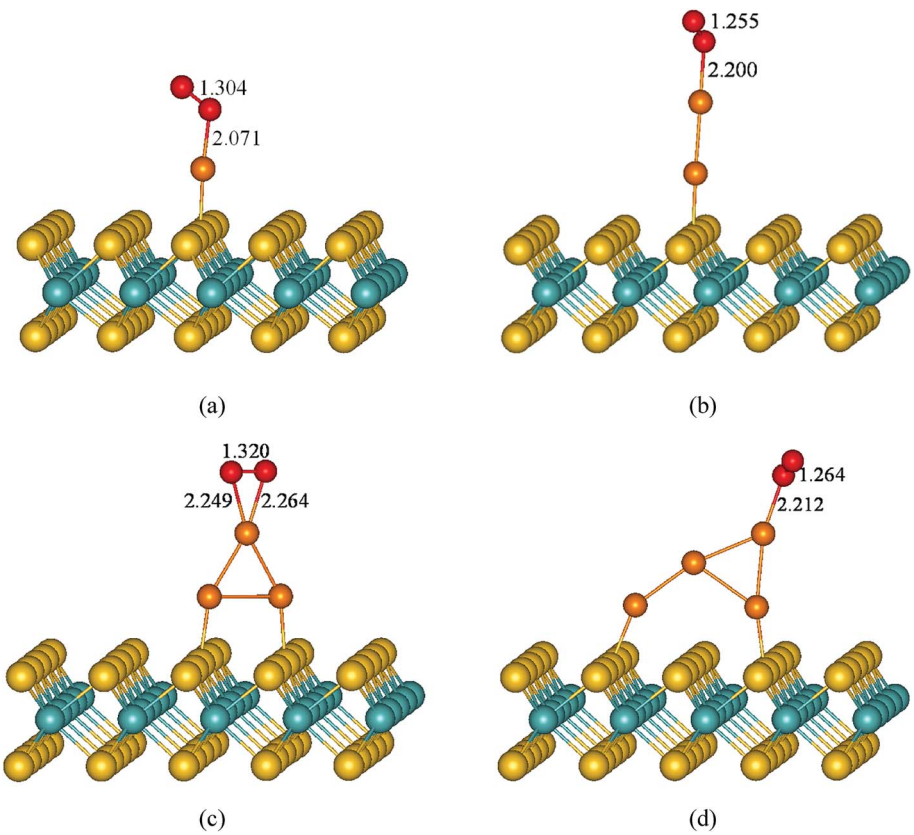


Fig. 6 Optimized structures of $O_2$ adsorbed on the most stable supported $Au_n$ ($n$ = 1–4) clusters. Color coding: orange, Au atoms; yellow, S atoms; cyan, Mo atoms; red, O atoms. Selected bond lengths are given in angstroms.

 

alternation as a function of the number of gold atoms. This phenomenon has been reported for $O_2$ molecule adsorption on the free gold clusters.[73–75]

To gain more insight into the origin of the activity of $Au_n$ ($n$ = 1–4)/$MoS_2$, we observed the electronic structures of $O_2$ adsorption on $Au_n$ ($n$ = 1–4)/$MoS_2$ systems. It is well-known that the singly occupied molecular orbital (SOMO) and the unoccupied one of the $O_2$ triplet ground state are both antibonding 2π* orbital. The spin-up 2π* orbital of free $O_2$ is occupied and located below the Fermi level, while the spin-down 2π* orbital of that is unoccupied and located above the Fermi level. We present the partial density of states (PDOS) projected on $O_2$ molecule and supported $Au_n$ ($n$ = 1–4) clusters in Fig. 7. Clearly, when $O_2$ interacts with supported $Au_n$ ($n$ = 1–4) clusters, the 5d and 6s state of Au atom is mixed with 1π and 2π* orbitals of the adsorbed $O_2$, indicating bonding of Au and $O_2$. Now the spin-down 2π* orbital of adsorbed $O_2$ appears partial population, indicated charge transfer occurring from the supported Au atom to the antibonding 2π* orbital of the adsorbed $O_2$, result in stretching of the O–O bond and the catalytic activation of $O_2$ molecule (Fig. 6). Furthermore, the charge distribution of adsorbed $O_2$, its neighbor Au atoms and $Au_n$ ($n$ = 1–4) clusters were calculated using Bader charge analysis, as listed in Table 4. The charge values of the supported $Au_n$ ($n$ = 1–4) clusters before $O_2$ adsorption are in the range of $-0.09e$ to $-0.11e$ except virtually zero for $Au_3$ cluster. After adsorption of $O_2$ molecule, more electrons are transferred from supported gold clusters to $O_2$ molecule, result in supported gold clusters become positive charge in the range of $+0.11e$ to $+0.35e$. Further atomic Bader charge analysis (Table 4) shows that the values of charge obtained by $O_2$ molecule mainly come from its neighboring Au atom which bonded to $O_2$ molecule. It also can be seen clearly from the electron charge density difference of $O_2$/$Au_n$ (1–4)/$MoS_2$ (Fig. 8). The isosurface of an excess of the electron density is mainly localized on $O_2$, while the plot of the electron density loss is on the Au atom directly interacting with $O_2$ molecule. This is consistent with above analysis of charge transfer from the supported neighboring gold clusters to $O_2$ molecule. Therefore, it is very clear that adsorption and activation of $O_2$ molecule are strongly influenced by the top Au atom which holds more negative charge. In addition, the values of charge obtained by $O_2$ molecule from supported $Au_1$ ($-0.39e$) and $Au_3$ clusters ($-0.38e$) are larger than that from supported $Au_2$ cluster ($-0.14e$) and $Au_4$ cluster ($-0.18e$), which are responsible for better catalytic activation of the adsorbed oxygen molecule. Note that from electron charge density difference (Fig. 8) there is more electron density localized on the $O_2$/$Au_n$ ($n$ = 1, 3)/$MoS_2$

Table 4 Bader charges of gold clusters ($Au_n$), neighboring gold atom (Au) and oxygen molecule

| | Substrate without $O_2$ | | Substrate with $O_2$ | | |
|---|---|---|---|---|---|
| | $\Delta Q(Au_n)$ | $\Delta Q^a$(Au) | $\Delta Q(Au_n)$ | $\Delta Q^b$(Au) | $\Delta Q(O_2)$ |
| $Au_1/MoS_2$ | −0.09 | −0.09 | +0.35 | +0.35 | −0.39 |
| $Au_2/MoS_2$ | −0.11 | −0.19 | +0.11 | +0.23 | −0.14 |
| $Au_3/MoS_2$ | +0.01 | −0.13 | +0.25 | +0.30 | −0.38 |
| $Au_4/MoS_2$ | −0.10 | −0.24 | +0.16 | +0.20 | −0.18 |

[a] $\Delta Q$(Au) and. [b] $\Delta Q$(Au) represent the charge value of the top Au atom which prefer to interact with $O_2$, respectively.

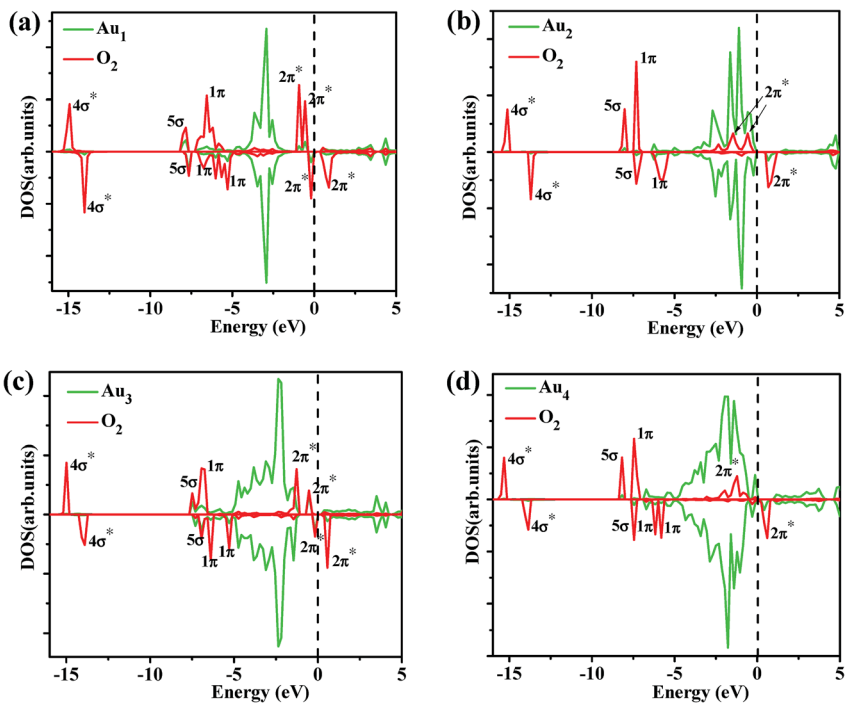


Fig. 7 Partial DOSs projected on the $O_2$ molecule and $Au_n$ ($n$ = 1–4) clusters of $O_2$ adsorption on $Au_1/MoS_2$ (a), $Au_2/MoS_2$ (b), $Au_3/MoS_2$ (c), and $Au_4/MoS_2$ (d). The vertical dashed line indicates the position of the Fermi level, taken as zero energy.

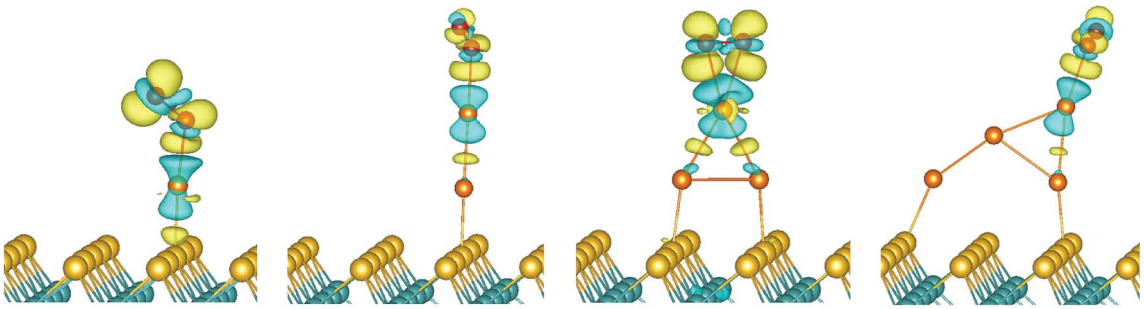


Fig. 8 Isosurfaces plot of the electron charge density difference for $O_2$ molecule on (a) $Au_1/MoS_2$, (b) $Au_2/MoS_2$, (c) $Au_3/MoS_2$, (d) $Au_4/MoS_2$, *i.e.*, $\rho_{tot}(O_2/Au_n/MoS_2) - \rho_{tot}(O_2) - \rho_{tot}(Au_n/MoS_2)$. The contours shown are at $\pm 0.003$ e Å$^{-3}$, respectively. Blue regions correspond to electron loss, and yellow ones correspond to electron accumulation.

systems with odd number of Au atoms than that on the $O_2/Au_n$ ($n$ = 2, 4)/$MoS_2$ systems with even number of Au atoms. This phenomenon corresponds to the above analysis of charge transfer from the supported gold clusters to $O_2$ molecule.

## 4 Conclusions

In the present work, we studied the structures, electronic properties and catalytic properties of $Au_n$ ($n$ = 1–4) clusters supported on monolayer $MoS_2$ using DFT calculations with and without the inclusion of van der Waals (vdW) forces, including PBE, PBE-D2, PBE-D3 and optB86b-vdW methods. We found that all $Au_n$ ($n$ = 1–4) clusters are preferentially vertically adsorbed on monolayer $MoS_2$ by Au–S bonds. The relative stability of $Au_n$ ($n$ = 1–4) clusters in gas phase is not preserved after landing on the monolayer $MoS_2$, indicating a possible way to stabilize the unstable clusters in the gas phase by choosing a suitable support from a thermodynamical point of view. The van der Waals correction increased the adsorption energies for all supported $Au_n$ ($n$ = 1–4) clusters with the relative order of adsorption energies of $E_{ads}$(PBE-D2) > $E_{ads}$(PBE-D3) > $E_{ads}$(optB86b-vdW) > $E_{ads}$(PBE). The van der Waals effects make the major corrections to the adsorption energies, and can also change the order of stability and the energy differences of various deposition configurations. The Bader charge analysis shows that, although the directions of charge transfer is from supported monolayer $MoS_2$ to supported $Au_n$ ($n$ = 1–4) clusters for all adsorption configurations, the top Au atoms far from the monolayer $MoS_2$ hold main negative charge whereas most of Au atoms at the interface become positive charged. It is demonstrated that the excess of the negative charges obtained by the top Au atom can considerably promote the adsorption and catalytic activation of $O_2$ on the supported $Au_n$ ($n$ = 1–4) clusters, due to the charge transfer occurring from the top Au atom to the $O_2$ $2\pi^*$ antibonding orbital, result in the elongation of the O–O bond and activation of $O_2$. Furthermore, our results represent better adsorption properties and catalytic activities of adsorbed $O_2$ on supported $Au_1$ and $Au_3$ clusters with magnetic properties, with respect to that on supported $Au_2$ and $Au_4$ clusters with nonmagnetic properties. The current study provides further insight into the adsorption and catalysis properties of small $Au_n$ ($n$ = 1–4) clusters supported on monolayer $MoS_2$, in which play a crucial role in the activation of $O_2$. More works are necessary to study the structure and the electronic properties to clearly see whether the number-dependent adsorption properties still holds when larger $Au_n$ nanocluster ($n$ > 4) supported on monolayer $MoS_2$

## Conflicts of interest

There are no conflicts to declare.

## Acknowledgements

This work was supported by National Natural Science Foundation of China (Grant No. 21403094, 21373048), and the Independent Research Project of State Key Laboratory of Photocatalysis on Energy and Environment (No. 2014A02). We are grateful for the generous allocation of computer time on the National Supercomputer Center in Guangzhou houses Tianhe-2.

## References

1 C. R. Henry, *Surf. Sci. Rep.*, 1998, **31**, 231–233.
2 G. Ertl and H. J. Freund, *Phys. Today*, 1999, **52**, 32–38.
3 B. Yoon, H. Hakkinen, U. Landman, A. S. Worz, J. M. Antonietti, S. Abbet, K. Judai and U. Heiz, *Science*, 2005, **307**, 403–407.
4 C. Zhang, B. Yoon and U. Landman, *J. Am. Chem. Soc.*, 2007, **129**, 2228–2229.
5 H. Y. Kim, H. M. Lee and G. Henkelman, *J. Am. Chem. Soc.*, 2012, **134**, 1560–1570.
6 Z. P. Liu, S. J. Jenkins and D. A. King, *Phys. Rev. Lett.*, 2005, **94**, 196102.
7 Q. Fu, H. Saltsburg and M. Flytzani-Stephanopoulos, *Science*, 2003, **301**, 935–938.
8 T. Mark, B. G. Vladimir, P. H. V. Owain, A. Pavel, B. G. Angel, S. T. Mintcho, F. G. J. Brian and M. L. Richard, *Nature*, 2008, **454**, 981–983.

9 H. Falsig, B. Hvolbaek, I. S. Kristensen, T. Jiang, T. Bligaard, C. H. Christensen and J. K. Nørskov, *Angew. Chem., Int. Ed.*, 2008, **120**, 4913–4917.
10 H. Häkkinen, S. Abbet, A. Sanchez, U. Heiz and U. Landman, *Angew. Chem., Int. Ed.*, 2003, **42**, 1297–1300.
11 A. Roldán, S. González, J. M. Ricart and F. Illas, *ChemPhysChem*, 2009, **10**, 348–351.
12 B. Yoon, P. Koskinen, B. Huber, O. Kostko, B. von Issendorff, H. Hakkinen, M. Moseler and U. Landman, *ChemPhysChem*, 2007, **8**, 157–161.
13 N. Lopez and J. K. Nørskov, *J. Am. Chem. Soc.*, 2002, **124**, 11262–11263.
14 I. N. Remediakis, N. Lopez and J. K. Nørskov, *Angew. Chem., Int. Ed.*, 2005, **117**, 1858–1860.
15 B. Yoon, H. Häkkinen, U. Landman, A. S. Wörz, J.-M. Antonietti, S. Abbet, K. Judai and U. Heiz, *Science*, 2005, **307**, 403–407.
16 Z. P. Liu, X. Q. Gong, J. Kohanoff, C. Sanchez and P. Hu, *Phys. Rev. Lett.*, 2003, **91**, 266102.
17 L. M. Molina and B. Hammer, *J. Chem. Phys.*, 2005, **123**, 161104.
18 A. Roldán, J. M. Ricart, F. Illas and G. Pacchioni, *J. Phys. Chem. C*, 2010, **114**, 16973–16978.
19 D. Matthey, J. G. Wang, S. Wendt, J. Matthiesen, R. Schaub, E. Lægsgaard, B. Hammer and F. Besenbacher, *Science*, 2007, **315**, 1692–1696.
20 S. Laursen and S. Linic, *Phys. Rev. Lett.*, 2006, **97**, 026101.
21 B. T. Teng, J.-J. Lang, X. D. Wen, C. Zhang, M. Fan and H. G. Harris, *J. Phys. Chem. C*, 2013, **117**, 18986–18993.
22 G. J. Hutchings, M. S. Hall, A. F. Carley, P. Landon, B. E. Solsona, C. J. Kiely, A. Herzing, M. Makkee, J. A. Moulijn, A. Overweg, J. C. Fierro-Gonzalez, J. Guzman and B. C. Gates, *J. Catal.*, 2006, **242**, 71–81.
23 L. Fu, N. Q. Wu, J. H. Yang, F. Qu, D. L. Johnson, M. C. Kung, H. H. Kung and V. P. Dravid, *J. Phys. Chem. B*, 2005, **109**, 3704–3706.
24 S. Stankovich, D. A. Dikin, G. H. B. Dommett, K. M. Kohlhaas, E. J. Zimney, E. A. Stach, R. D. Piner, S. T. Nguyen and R. S. Ruoff, *Nature*, 2006, **442**, 282–286.
25 E. Gracia-Espino, G. Hu, A. Shchukarev and T. Wagberg, *J. Am. Chem. Soc.*, 2014, **136**, 6626–6633.
26 P. Vogt, P. D. Padova, C. Quaresima, J. Avila, E. Frantzeskakis, M. C. Asensio, A. Resta, B. Ealet and G. L. Lay, *Phys. Rev. Lett.*, 2012, **108**, 155501.
27 G. Kim, A. R. Jang, H. Y. Jeong, Z. Lee, D. J. Kang and H. S. Shin, *Nano Lett.*, 2013, **13**, 1834–1839.
28 M. Gao, A. Lyalin and T. Taketsugu, *J. Phys. Chem. C*, 2012, **116**, 9054–9062.
29 T. Liao, Z. Sun and S. X. Dou, *ACS Appl. Mater. Interfaces*, 2017, **9**, 8255–8262.
30 L. Sheng, T. Liao, L. Kou and Z. Sun, *Mater. Today Energ.*, 2017, **3**, 32–39.
31 T. Liao, Z. Sun, C. Sun, S. X. Dou and D. J. Searles, *Sci. Rep.*, 2014, **4**, 6256.
32 A. K. Geim and K. S. Novoselov, *Nat. Mater.*, 2007, **6**, 183–191.
33 A. K. Geim, *Science*, 2009, **324**, 1530–1534.
34 K. F. Mak, C. Lee, J. Hone, J. Shan and T. F. Heinz, *Phys. Rev. Lett.*, 2010, **105**, 136805.
35 M. Chhowalla, H. S. Shin, G. Eda, L. J. Li, K. P. Loh and H. Zhang, *Nat. Chem.*, 2013, **5**, 263–275.
36 J. Zhu, H. Zhang, Y. Tong, L. Zhao, Y. Zhang, Y. Qiu and X. Lin, *Appl. Surf. Sci.*, 2017, **419**, 522–530.
37 Y. Shi, J. Wang, C. Wang, T.-T. Zhai, W. J. Bao, J. J. Xu, X. H. Xia and H. Y. Chen, *J. Am. Chem. Soc.*, 2015, **137**, 7365–7370.
38 A. R. Puigdollers, P. Schlexer and G. Pacchioni, *J. Phys. Chem. C*, 2015, **119**, 15381–15389.
39 J. Carrasco, W. Liu, A. Michaelides and A. Tkatchenko, *J. Chem. Phys.*, 2014, **140**, 084704.
40 G. Kresse and J. Hafner, *Phys. Rev. B: Condens. Matter Mater. Phys.*, 1994, **49**, 14251–14269.
41 G. Kresse and J. Furthmüller, *Comput. Mater. Sci.*, 1996, **6**, 15–50.
42 G. Kresse and J. Furthmüller, *Phys. Rev. B: Condens. Matter Mater. Phys.*, 1996, **54**, 11169–11186.
43 P. E. Blöchl, *Phys. Rev. B: Condens. Matter Mater. Phys.*, 1994, **50**, 17953–17979.
44 G. Kresse and D. Joubert, *Phys. Rev. B: Condens. Matter Mater. Phys.*, 1999, **59**, 1758–1775.
45 J. P. Perdew, K. Burke and M. Ernherhof, *Phys. Rev. Lett.*, 1996, **77**, 3865–3868.
46 P. Joensen, E. D. Crozier, N. Alberding and R. F. Frindt, *J. Phys. C: Solid State Phys.*, 1987, **20**, 4043–4053.
47 D. Le, T. B. Rawal and T. S. Rahman, *J. Phys. Chem. C*, 2014, **118**, 5346–5351.
48 Q. Chen, Y. Ouyang, S. Yuan, R. Li and J. Wang, *ACS Appl. Mater. Interfaces*, 2014, **6**, 16835–16840.
49 D. Ma, Y. Tang and G. Yang, *Appl. Surf. Sci.*, 2015, **328**, 71–77.
50 C. Ataca and S. Ciraci, *J. Phys. Chem. C*, 2011, **115**, 13303–13311.
51 G. Zanti and D. Peeters, *Theor. Chem. Acc.*, 2013, **132**, 1300.
52 H. M. Lee and K. S. Kim, *Chem.–Eur. J.*, 2012, **18**, 13203–13207.
53 S. Nosé, *J. Chem. Phys.*, 1984, **81**, 511–519.
54 J. Zhu, H. Zhang, Y. W. Tong, Y. W. Tong, C. X. Wang, B. Wang, X. Huang and Y. F. Zhang, *J. Chem. Phys.*, 2016, **144**, 174706.
55 J. Zhu, H. Zhang, L. Zhao, W. Xiong, X. Huang, B. Wang and Y. F. Zhang, *Appl. Surf. Sci.*, 2016, **138**, 213–222.
56 S. Grimme, *J. Comput. Chem.*, 2006, **27**, 1787–1799.
57 S. Grimme, J. Antony, S. Ehrlich and H. Krieg, *J. Chem. Phys.*, 2010, **132**, 154104.
58 M. Dion, H. Rydberg, E. Schröder, D. C. Langreth and B. I. Lundqvist, *Phys. Rev. Lett.*, 2004, **92**, 246401.
59 C. L. Cleveland, U. Landman, T. G. Schaaff, M. N. Shafigullin, P. W. Stephens and R. L. Whetten, *Phys. Rev. Lett.*, 1997, **79**, 1873–1876.
60 T. G. Schaaff, M. N. Shafigullin, J. T. Khoury, I. Vezmar, R. L. Whetten, W. G. Cullen, P. N. First, C. Gutiérrez-Wing, J. Ascensio and M. J. Jose-Yacamán, *J. Phys. Chem. B*, 1997, **101**, 7885–7891.
61 K. J. Taylor, C. L. Pettiette-Hall, O. Cheshnovsky and R. E. Smalley, *J. Chem. Phys.*, 1992, **96**, 3319–3329.

62 K. Koga, H. Takeo, T. Ikeda and K. Ohshima, *Phys. Rev. B: Condens. Matter Mater. Phys.*, 1998, **57**, 4053–4062.
63 V. A. Spasov, Y. Shi and K. M. Ervin, *Chem. Phys.*, 2000, **262**, 75–91.
64 B. Palpant, B. Prével, J. Lérme, E. Cottancin, M. Pellarin, M. Treilleux, A. Perez, J. L. Vialle and M. Broyer, *Phys. Rev. B: Condens. Matter Mater. Phys.*, 1998, **57**, 1963–1970.
65 M. S. Liao, J. D. Watts and M. J. Huang, *J. Phys. Chem. C*, 2014, **118**, 21911–21927.
66 J. Wang, G. Wang and J. Zhao, *Phys. Rev. B: Condens. Matter Mater. Phys.*, 2002, **66**, 035418.
67 X. B. Li, H. Y. Wang, X. D. Yang, Z.-H. Zhu and Y. J. Tang, *J. Chem. Phys.*, 2007, **126**, 084505.
68 J. L. Jules and J. R. Lombardi, *J. Phys. Chem. A*, 2003, **107**, 1268–1273.
69 R. F. W. Bader, *Chem. Rev.*, 1991, **91**, 893–928.
70 G. Henkelman, A. Arnaldsson and H. Jónsson, *Comput. Mater. Sci.*, 2006, **36**, 354–360.
71 W. Tang, E. Sanville and G. Henkelman, *J. Phys.: Condens. Matter*, 2009, **21**, 084204.
72 Y. Shi, J. K. Huang, L. Jin, Y. T. Hsu, S. F. Yu, L. J. Li and H. Y. Yang, *Sci. Rep.*, 2013, **3**, 1839.
73 A. Lyalin and T. Taketsugu, *J. Phys. Chem. C*, 2009, **113**, 12930–12934.
74 B. Yoon, H. Häkkinen and U. Landman, *J. Phys. Chem. A*, 2003, **107**, 4066–4071.
75 X. L. Ding, Z. Y. Li, J. L. Yang, J. G. Hou and Q. S. Zhu, *J. Chem. Phys.*, 2004, **120**, 9594–9600.